Astronomy
& Astrophysics

LETTER TO THE EDITOR

Eruptions of two flux ropes observed by SDO and STEREO

L. P. Li, and J. Zhang

Key Laboratory of Solar Activity, National Astronomical Observatories, Chinese Academy of Sciences, 100012 Beijing, PR China
e-mail: lepingli@nao.cas.cn

ABSTRACT

Aims. We report for the first time the hot and cool components of two flux ropes simultaneously observed by SDO and STEREO, and the relationship between the flux rope eruptions and the coronal mass ejection (CME).
Methods. Employing SDO and STEREO A and B observations, we investigated the eruptive event of two flux ropes and their associated activities in active region (AR) 11402 on January 23, 2012.
Results. In SDO/AIA 94 Å (∼6.4 MK) and 131 Å (∼10 MK) images, a twisted flux rope appeared from 00:44 UT, which was located in AR 11402. Another longer saddle-shaped flux rope, with twisted fine structures, appeared 25 min later. This was located across the two ARs 11401 and 11402. These two flux ropes initially rose rapidly, then slowly, and finally were again accelerated fast. The two flux ropes are also identified in the STEREO A and B 195 Å (∼1.4 MK), 304 Å (0.06–0.08 MK), 284 Å (∼1.8 MK), and 171 Å (∼1.0 MK) observations. We suggest that the flux ropes may have both hot and cool components. Investigating the flux rope eruptions with their associated CME, we find that the erupting flux ropes are co-spatial with the CME bright core and the expanding overlying flux loops with the CME bright front.

Key words. Sun: filaments, prominences – Sun: flares – Sun: coronal mass ejections (CMEs) – sunspots

1. Introduction

Coronal mass ejections (CMEs) are large-scale magnetized plasma eruptions from the solar atmosphere that release a huge amount of mass and magnetic flux into the interplanetary space and may cause severe disturbances of the space environment. They correspond to a sudden, explosive release of free magnetic energy stored in the previously quasi-equilibrium, twisted/sheared coronal magnetic fields (Gibson et al. 2006), and represent a large-scale rearrangement of the coronal magnetic structures (Forbes et al. 2006). CMEs usually occur in solar corona above or in the neighborhood of active regions (ARs), and are frequently accompanied by flares, soft X-ray sigmoids, and filament eruptions.

The flux rope, which is considered to be a fundamental structure underlying CMEs, is a set of magnetic field lines that is wound around an axis. This is an important topic in solar terrestrial research. An isolated flux rope, referred to as a magnetic cloud, was first directly detected from near-Earth insitu solar wind observations (Burlaga et al. 1981). Using the Solar and Heliospheric Observatory (SOHO) data, Dere et al. (1999) and Krall et al. (2001) observed internal helical structures of CMEs, and described them as a flux rope. Liu et al. (2003) studied an M 3.0 flare on July 15, 2002, and presented observational evidence of a flux rope eruption. Using multi-instrument data, Raouafi (2009) also found observational evidence for a twisted flux rope. Recently, Cheng et al. (2011) presented an unambiguous observation of a flux rope in the low corona, and Zhang et al. (2012) reported a magnetic flux rope as a hot channel prior to and during a solar eruption from Solar Dynamic Observatory/Atmospheric Imaging Assembly (SDO/AIA; Lemen et al. 2012) observations.

Considerable effort has also been made in numerical simulations to study the formation and dynamic behavior of magnetic flux ropes (e.g., Forbes 1995; Lin et al. 1998; Aulanier et al. 2010). Amari et al. (2000) simulated the evolution of a flux rope and noticed that it plays a crucial role in the process of a CME. Török & Kliem (2003, 2005) studied the instability of a flux rope and proposed that the kink and/or torus instability can trigger a CME. Fan (2005) and Fan & Gibson (2007) used the flux rope to model the loss of confinement and the eruption of a flux rope emerging quasi-statically into a preexisting coronal arcade field. Furthermore, employing nonlinear force-free field extrapolation, Guo et al. (2010) and Canou & Amari (2010) each found a flux rope along the polarity inversion line (PIL).

On January 23, 2012, a CME was recorded by SOHO/LASCO C2 from 03:24 UT, and an associated eruptive event was observed in AR 11402. In this Letter, we study the evolution of the eruptive event and its relationship with the CME. The data and observations are described in Sect. 2. We present the results in Sect. 3 and the conclusions and discussion in Sect. 4.

2. Data and observations

The SDO/AIA is a set of normal incidence imaging telescopes designed to acquire images of the solar atmosphere at ten wavelength bands. In this study, we used SDO/AIA images with a time cadence and spatial resolution of 12 s and 1.2″ to investigate the evolution of the eruptive event, and SDO/Helioseismic and Magnetic Imager (HMI; Schou et al. 2012) line of sight (LOS) magnetograms with a time cadence and spatial resolution of 45 s and 1.0″ to study the evolution of the AR magnetic fields. Using Solar Terrestrial Relations Observatory (STEREO)/SECCHI and SOHO/LASCO observations, we researched the kinematics of the eruptive event and the CME. The spatial resolutions and time cadences of SECCHI/EUVI A and B 195 Å images are 3.2″ and 5 min, and COR1 images, 30″ and 5 min. Moreover, we employed
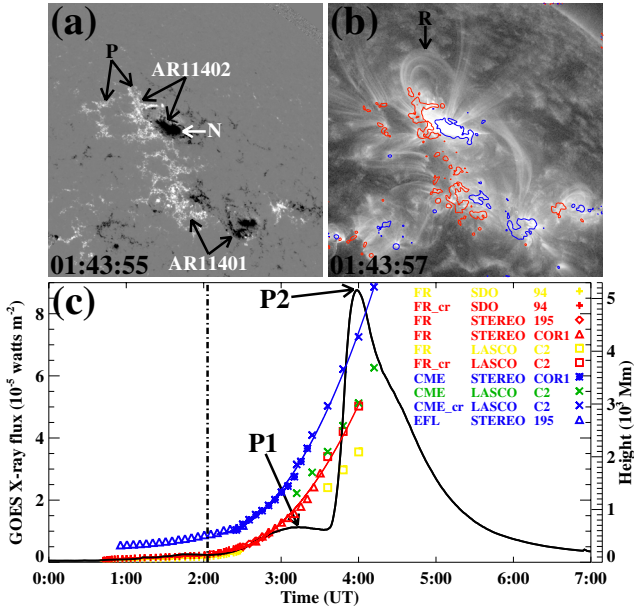
Fig. 1. SDO/HMI LOS magnetogram **a)** and SDO/AIA 131 Å image **b)** showing the AR information. N in **a)** indicates a negative sunspot, P in **a)** diffused positive magnetic fields, blue and red contours in **b)** the LOS magnetic flux densities of –200 G and 200 G, and R in **b)** flux ropes. The field of view (FOV) is 310″ × 310″. **c)** The GOES-15 1–8 Å soft X-ray flux (the black solid curve). P1 and P2 mark two peaks. The colored signs represent the heights of the flux ropes and CME (see text for details), and the red and blue lines denote the second-order polynomial fits to CME bright core and front. FR represents the flux ropes and EFL the expanding flux loops. The terms with "cr" mean the heights after correction for the projection effect.

Geostationary Operational Environmental Satellite (GOES) data to explore the variation of the soft X-ray flux.

3. Results

The AR 11402 was located at heliographic position N29 W36 on January 23, 2012. Figure 1a displays a SDO/HMI LOS magnetogram showing the general information of the AR, which consists of a main negative magnetic field N in the southwest, and extended diffused positive magnetic fields P in the northeast. To the southwest of the AR, there is another AR 11401, located at N16 W39. Figure 1b presents an AIA 131 Å image shows an erupting coronal structure denoted by R that has a twisted configuration. Cheng et al. (2011) and Zhang et al. (2012) considered this kind of coronal structure as observational evidence of a flux rope. Following their consideration, we use the term flux rope to represent a twisted coronal structure, and the term flux loop to represent an untwisted coronal structure. Figure 1c shows the GOES-15 1–8 Å soft X-ray flux (the black solid line), from which two successive M-class flares are detected. The first one, accompanying the flux rope eruption (see Fig. 1b), is an M 1.1 flare that began at 02:00 UT and peaked at 03:13 UT (see P1 in Fig. 1c), while the second one, associated with a filament eruption in AR 11402, is an M 8.7 flare with a peak time of 03:58 UT (see P2 in Fig. 1c). Moreover, the soft X-ray flux rose slowly from 00:39 UT before the M 1.1 flare. In this letter, we study the M 1.1 flare and its associated eruptions.

Figures 2a–2c and 2d–2f separately show AIA 131 Å and 94 Å base difference images displaying two erupting flux ropes. The red and blue contours in Fig. 2 enclose the positive and
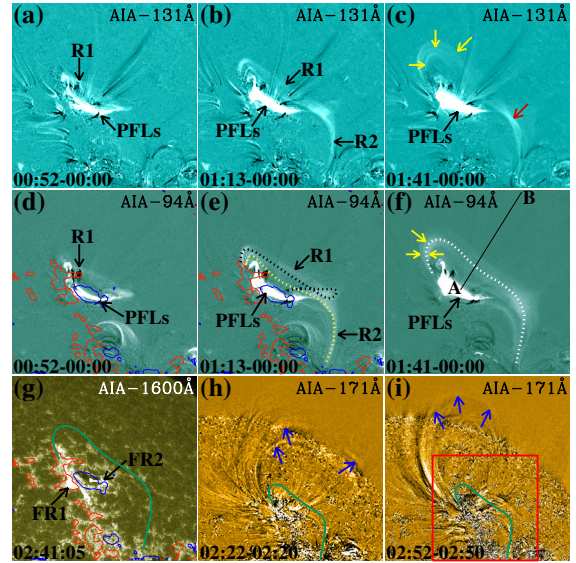

Fig. 2. Time series of SDO/AIA 131 Å (**a**–**c**) and 94 Å (**d**–**f**) base difference images displaying eruptions of the two flux ropes R1 and R2. An AIA 1600 Å image (**g**) illustrating two flare ribbons, FR1 and FR2, and two AIA 171 Å running difference images (**h**–**i**), showing the flux loop expansion. PFLs represents post-flare loops, and blue and red contours the LOS magnetic flux densities of –150 G and 150 G. The yellow arrows in **c**) and **f**) denote flux ropes, the red arrow in **c**) marks twisted structures, and blue arrows in **h**)–**i**) indicates the expansion. The curves in **e**)–**i**) mark flux ropes, and the black line AB in **f**) the position for time slice evolution displayed in Fig. 3. The FOV of **h**)–**i**) is 420″ × 420″. The red window in **i**) represents the FOV of **a**)–**g**), 240″ × 240″.

negative magnetic fields, respectively. The first flux rope R1 (see Figs. 2a–2f) appeared from 00:39 UT as a twisted sigmoidal structure (see the black dotted curve in Fig. 2e), and then rose northwestward. It was located in AR 11402. Thirty minutes later (01:09 UT), another flux rope R2 (see Figs. 2b and 2e) appeared to the south of R1 and also rose toward the northwest. The second flux rope R2 is a longer twisted saddle-like structure (see the yellow dotted curve in Fig. 2e). This was located across the two ARs 11401 and 11402. The northeastern foot of R2 is near the northeastern foot of R1; however, the southwestern foot of R2 lies to the south of the southwestern foot of R1. Afterward, these two flux ropes erupted outward from twisted structures to semi-circular ones while their footpoints remained fixed. During the eruption, fine structures of R2, denoted by three yellow arrows in Figs. 2c and 2f, are detected. These fine structures are twisted together and are marked by a red arrow in Fig. 2c.

Accompanying the flux rope eruptions, post-flare loops (see PFLs in Fig. 2) appeared shortly before the flux ropes. This implies that the flux ropes were invisible for the first part of the eruptions. Figure 2g displays an AIA 1600 Å image showing two flare ribbons FR1 and FR2 of the M 1.1 flare. The eastern ribbon FR1 is rooted in the diffused positive magnetic fields P and the western ribbon FR2 in the negative magnetic fields N. We overlay the general structure of R2 at 01:41 UT (see the white dotted line in Fig. 2f) in Fig. 2g as a green curve; the flux rope is located upon the PIL and is almost parallel to the flare ribbons.

The two flux ropes are detected only in the AIA two hottest passband (~6.4 MK at 94 Å and ~10 MK at 131 Å) images. From the cooler AIA 171 Å (~1 MK), 193 Å (~1.6 MK), and 211 Å (~2 MK) data, we find that the expansion of the flux loops overlies the flux ropes. Figures 2h and 2i display the AIA 171 Å running difference images that show the expansion,
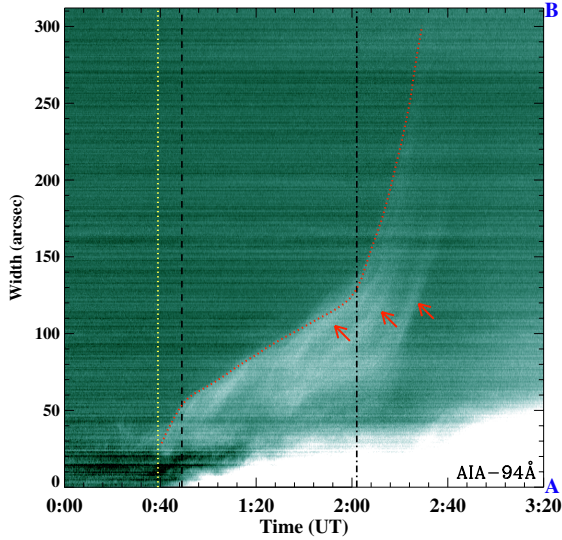
Fig. 3. Time slice of a series of SDO/AIA 94 Å base difference images along the black line AB displayed in Fig. 2f. The red dotted curve marks the front of the erupting flux ropes. Three vertical lines separate the three phases of the eruptions, and the three red arrows denote the flux ropes.

Fig. 4. Time series of STEREO-A 195 Å (**a**–**c**), 304 Å (**g**), and STEREO-B 195 Å (**d**–**f**) running difference images illustrating the eruptions of flux ropes R1 and R2. Composites of STEREO EUVI 195 Å and COR1 white-light running difference images (**h**), and SDO/AIA 94 Å and SOHO/LASCO C2 running difference images (**i**), displaying the relationship between flux rope eruptions and a CME. R in **i**) denotes flux ropes, and D in **c**) and **h**) a dark region. The red and blue curves in **b**) describe R1 and R2, and the green arrows the expanded flux loops. The colored triangles and diamonds in **c**) and **f**) separately represent three positions of R1 and R2. The FOV of **d**)–**f**), **h**) and **i**) are $1.0 R_\odot \times 1.0 R_\odot$, $2.7 R_\odot \times 2.7 R_\odot$ and $6.2 R_\odot \times 6.2 R_\odot$. The green window in **h**) denotes the FOV of **a**)–**c**) and **g**), $1.0 R_\odot \times 1.0 R_\odot$.

which was first clearly observed in images from 02:09 UT, marked by blue arrows. The red window in Fig. 2i represents the fields of view (FOV) of Figs. 2a–2g, and the green curves in Figs. 2h and 2i plots R2 in Fig. 2f. Apparently, the expanding flux loops are perpendicular to the erupting flux ropes.

Along the black solid line AB in Fig. 2f, we made a time slice of a series of AIA 94 Å base difference images, which we show in Fig. 3. Three fine structures of flux ropes with similar rising trends, marked by three red arrows, are detected. The red dotted line describes the front of the erupting flux ropes. It shows that the eruption process can be divided into three distinct phases: a fast rise, a slow rise, and a fast acceleration. The flux ropes began to rise from 00:39 UT (see the yellow dotted line) with an average velocity of 40.5 km s^{-1}. From 00:49 UT (see the dashed line), the flux ropes rose at a comparatively lower speed of 13 km s^{-1}, and lasted for 75 min. From 02:00 UT (see the dash-dotted line), the flux ropes accelerated significantly, and propagated at a higher mean speed of 76.6 km s^{-1}. We plot the heights of flux rope front from the AR 11402 as yellow pluses in Fig. 1c. Assuming that the flux ropes erupted radially outward, we corrected for the projection effect to obtain the corrected heights; they are displayed in Fig. 1c as red pluses. It seems that the flux ropes and the soft X-ray flux have similar rising trends. Moreover, the beginning of the fast acceleration phase is identical to the onset of the M 1.1 flare.

Two flux ropes are also identified in both STEREO A and B observations. On January 23, 2012, the separation angle between STEREO A (B) and SDO was 108° (114°), and STEREO A and B, 138°. The AR 11402 was hence located at the northeastern (northwestern) limb of the STEREO A (B) images (see Fig. 4). Figures 4a–4c display SECCHI/EUVI-A 195 Å running difference images illustrating the northeastward eruption of two flux ropes, denoted also by R1 and R2, which were first detected at 02:25 UT. The R1, here, has a twisted structure (see the blue line in Fig. 4b), and R2 shows a twisted saddle-like structure (see the red line in Fig. 4b). Moreover, R2 has twisted fine structures, marked by two red arrows in Fig. 4c, and its southern foot is rooted to the south of the southern foot of R1. These
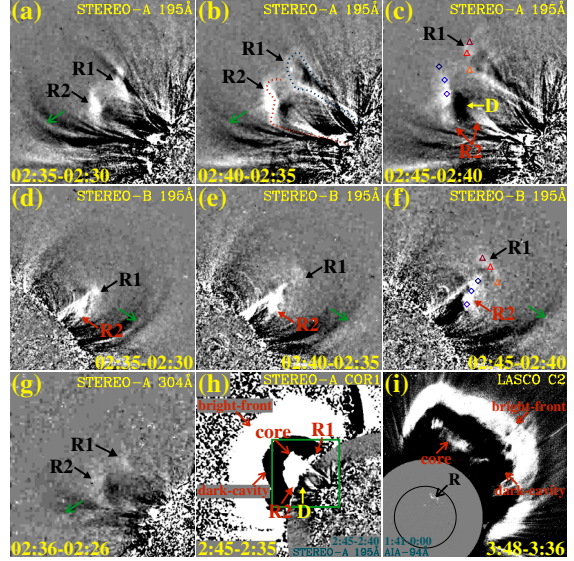
results are identical to those displayed in Fig. 2, suggesting the flux ropes R1 and R2 detected by STEREO are consistent with the flux ropes R1 and R2 observed by SDO. Comparing these with EUVI-A observations, we show simultaneous EUVI-B 195 Å running difference images in Figs. 4d–4f that display two bright structures. Using a routine called SCC_MEASURE from the solar software (SSW) library, we reconstructed the two flux ropes and found the two bright structures in Figs. 4d–4f are consistent with the two flux ropes (R1 and R2) in Figs. 4a–4c. Three colored triangles (diamonds) in Figs. 4c and 4f represent the three positions of the upper part of R1 (R2), and the same colored triangles (diamonds) plot the same positions of R1 (R2) separately observed by STEREO A and B. Based on the reconstruction, we found that the flux rope propagation observed by STEREO-A mostly represents the real propagation, therefore we employed the STEREO-A measurements as the real ones. R2 erupted at a mean speed and acceleration of 201 km s^{-1} and 15 m s^{-2}, and R1 moved out in sync with R2. We plot the heights of R2 from the AR as red diamonds in Fig. 1c. Apparently, the heights observed by STEREO are temporally and spatially consistent with those observed by SDO. This also indicates that these two flux ropes detected by STEREO and SDO are the same. The expansion of flux loops (see the green arrows) overlying the flux ropes are also identified from 00:55 UT, which is after the appearance (00:39 UT) of R1, but before the appearance (02:09 UT) of the expansion observed by SDO. We measured the heights of the expanding flux loops and mark them as blue triangles in Fig. 1c. The expanding flux loops began to accelerate in a similar way to the onset of the M 1.1 flare. The eruption of the flux ropes and the expansion of the overlying flux loops are

also observed in the STEREO 171 Å, 284 Å, and 304 Å images. Figure 4g shows an EUVI-A 304 Å example.

Associated with the flux rope eruptions, a CME was recorded by STEREO/COR1 beginning at 02:25 UT with a classic three-part structure: a bright front, a dark cavity, and a bright core. We display a composite of co-temporal EUVI-A 195 Å and COR1-A white-light running difference images in Fig. 4h, in which the green window represents the FOV of Figs. 4a–4c. Figure 4h shows that the CME bright core has fine structures that are spatially consistent with these two flux ropes, i.e., the western core corresponds to R1 and the eastern core to R2. Moreover, the CME bright front is spatially the same as the overlying expanding flux loops. We plot the heights of the CME bright core (front) from AR 11402 observed by COR1-A as red triangles (blue asterisks) in Fig. 1c. The kinematics of the flux ropes and CME also support the relationship between flux rope eruptions and CME. The CME bright core (front) propagated northeastward with an average velocity and acceleration of 395 (435) km s^{-1} and 94 (96) m s^{-2}, respectively. Figure 4i displays a composite of an AIA 94 Å base difference image, the inner one inside a black circle, and a LASCO C2 running difference image, the outer one. It also indicates that the CME is associated with the erupting flux ropes. We measured the heights of CME bright core and front from the AR and corrected for the projection effect assuming the CME propagated radially outward. We separately plot these measured (green X) and corrected (blue X) heights in Fig. 1c and note that the CME in LASCO C2 is consistent with that detected by STEREO/COR1. The measured (corrected) average speed of the CME bright core is 470 (665) km s^{-1}, and the velocity of the CME bright front is 648 (917) km s^{-1}.

Considering all observations (the colored signs) in Fig. 1c, we find that the flux ropes/CME bright core (expanding flux loops/CME bright front) erupted with an average velocity and acceleration of 360 (695) km s^{-1} and 67 (84) m s^{-2} (see the red and blue curves in Fig. 1c), respectively, during the fast acceleration phase. Both flux ropes (CME bright core) and expanding flux loops (CME bright front) have the similar rising trends; however, the expanding flux loops (CME bright front) seems to propagate slightly faster than the flux ropes (CME bright core), especially in the later stage.

4. Conclusions and discussion

Employing SDO and STEREO observations, we investigated the eruptive event of two flux ropes and their associated activities on January 23, 2012, and obtained the following results:

Two flux ropes are detected both in the SDO 94 Å and 131 Å and the STEREO A and B 195 Å, 304 Å, 171 Å, and 284 Å images. The first flux rope, located in an AR, is a twisted sigmoidal structure, and the other one, connecting two ARs, a longer saddle-like structure with a twisted fine structures. The eruptions have three phases: a fast rise, a slow rise, and a fast acceleration. During the eruptions, the footpoints of flux ropes remained fixed. Expansions of flux loops overlying the flux ropes are found in the SDO 171 Å, 193 Å, and 211 Å and the STEREO 195 Å, 304 Å, 171 Å, and 284 Å images. Both the flux rope eruptions and the flux loop expansions have rising trends similar to soft X-ray flux in the beginning, and accelerated fast when the associated flare began. The flux ropes are temporally and spatially consistent with the CME bright core, and the expanding overlying flux loops are the same as the CME bright front.

The observational evidence, such as the twisted structures, the fixed footpoints, and the associated flare and CME, supports the hypothesis that the coronal structures are magnetic flux ropes (Zhang et al. 2012). Two flux ropes with fine structures, not just one as reported in Zhang et al. (2012), were detected. However, as the northeastern foots of two flux ropes cannot well be separated, and two flux ropes moved out in sync with each other, we cannot exclude another possibility, i.e., that R1 and R2 are two parts of a same single (or joined) complicated flux rope. Flux ropes, therefore, may be complex magnetic flux systems. Flux ropes have been detected in SDO's two hottest passbands (Cheng et al. 2011, Zhang et al. 2012) and also in STEREO 195 Å and 284 Å (Vourlidas et al. 2012). Here, we report both results simultaneously for the first time. This shows that flux ropes may have both hot and cool components (Cheng et al. 2012). Because SDO hot passband images and STEREO images show material in different temperatures, the flux ropes, separately observed by SDO and STEREO, may represent different parts of the same structures. Our flux ropes were observed in the cooler passband observations from the STEREO telescopes, but not in the cooler passbands of SDO/AIA. This may be due to the different viewing directions of the different satellites. We first observationally studied the relationship between the flux rope eruptions and a CME. This can help us understand the CMEs without filament eruptions, and supports the CME models with magnetic flux ropes (e.g., Fan 2005; Fan & Gibson 2007; Aulanier et al. 2010). It is, therefore, reasonable to consider flux rope eruptions as CMEs in the inner corona (Cheng et al. 2011, 2012). However, the detailed characteristics of magnetic flux ropes are not clear yet. More observations and theoretical studies are needed.

References

Amari, T., Luciani, J. F., Mikic, Z., & Linker, J. 2000, ApJ, 529, L49
Aulanier, G., Török, T., Démoulin, P., & DeLuca, E. E. 2010, ApJ, 708, 314
Burlaga, L. F., Sittler, E., Mariani, F., & Schwenn, R. 1981, J. Geophys. Res., 86, 6673
Canou, A., & Amari, T. 2010, ApJ, 715, 1566
Cheng, X., Zhang, J., Liu, Y., & Ding, M. D. 2011, ApJ, 732, L25
Cheng, X., Zhang, J., Saar, S. H., & Ding, M. D. 2012, ApJ, 761, 62
Dere, K. P., Bruechner, G. E., Howard, R. A., Michels, D. J., & Delaboudinière, J. P. 1999, ApJ, 516, 465
Fan, Y. 2005, ApJ, 630, 543
Fan, Y., & Gibson, S. E. 2007, ApJ, 668, 1232
Forbes, T. G., & Priest, E. R. 1995, ApJ, 446, 377
Forbes, T. G., Linker, J. A., Chen, J., et al. 2006, Space Sci. Rev., 123, 251
Gibson, S. E., Fan, Y., Török, T., & Kliem, B. 2006, Space Sci. Rev., 124, 131
Guo, Y., Ding, M. D., Schmieder, B., et al. 2010, ApJ, 714, 343
Krall, J., Chen, J., Duffin, R. T., Howard, R. A., & Thompson, B. J. 2001, ApJ, 562, 1045
Lemen, J. R., Title, A. M., Akin, D. J., et al. 2012, Sol. Phys., 275, 17
Lin, J., Forbes, T. G., Isenberg, P. A., & Demoulin, P. 1998, ApJ, 504, 1006
Liu, Y., Jiang, Y. C., Ji, H. S., Zhang, H. Q., & Wang, H. M. 2003, ApJ, 593, L137
Raouafi, N.-E. 2009, ApJ, 691, L128
Schou, J., Scherrer, P. H., Bush, R. I., et al. 2012, Sol. Phys., 275, 229
Török, T., & Kliem, B. 2003, A&A, 406, 1043
Török, T., & Kliem, B. 2005, ApJ, 630, L97
Vourlidas, A., Syntelis, P., & Tsinganos, K. 2012, Sol. Phys., 280, 509
Zhang, J., Cheng, X., & Ding, M. D. 2012, Nature Commun., 3, 747